Near field CSAMT resistivity and model parameter determination

I. B. Ramaprasada Rao*,†, M. Venkata Chary†, Ram Raj Mathur† and S. Srinivas**

†Centre of Exploration Geophysics, Department of Geophysics, Osmania University, Hyderabad 500 007, India
**BHP Minerals, Tekunj, Udaipur 313 001, India

Cagniard resistivity approach in controlled source audio-frequency magnetotellurics/magnetotellurics (CSAMT/MT) data handling assumes a plane wave EM source. Hence, near field Cagniard's resistivity does not permit the determination of model parameters. This paper presents the study of near/transition field apparent resistivity over multi-layered media by resorting to near field apparent resistivity and examines the possibility of extracting model parameters from near field CSAMT data, which hitherto has been ignored or corrected, using the well-known Marquardt algorithm.

The per cent deviation ($\Delta\alpha\%$) between the true and fitted geoelectric parameters for a two-layer case increases with increase in ρ_2/ρ_1 when ($\rho_2 < \rho_1$) for all values of r/h_1, h_1 being the thickness of the first-layer and r the distance between the transmitter and receiver. When $r/h_1 \gg 1$, $\Delta\alpha\%$ is well below 15%. In case $\rho_2 > \rho_1$, the per cent deviation is within 5% when $\rho_2/\rho_1 > 20$ and $r/h_1 \geq 1$. Over a three-layer geoelectric section the per cent deviation is within the 'acceptable' limits for the geoelectric parameters studied. Thus, this paper shows a way to invert the near zone CSAMT data which is a necessity to probe deeper layers. However, the scheme has poorer resolvability in the case of three-layer A-type geoelectric section.

THE controlled source audio-frequency magnetotellurics (CSAMT) apparent resistivity differs considerably from magnetotellurics (MT) as the non plane wave effects have to be taken into consideration for near field conditions[1–3]. While the literature references[2,4–7] are numerous regarding the determination of earth structure from the inversion of MT data (plane wave solution), published studies on the inversion of CSAMT data in the entire spectrum of frequencies encroaching on to near field conditions are scarce. A comprehensive review of the theory of CSAMT indicates that the Cagniard apparent resistivity decreases monotonously with increase in frequency for the near field conditions and hence does not permit the determination of the earth structure. Precisely for this reason, Takakura[8], Ogawa and Takakura[9], Yamashita[10] and Bromley[11] reported CSAMT inversion leaving out the low frequency branch, thus losing vital information regarding deeper sections. Pris and Svetov[12] also presented interpretation of nomograms for near field geometric CSAMT soundings of a two-layer structure. Yamashita and Hallof[1], Bartel and Jacobson[13] and Rao *et al.*[3] presented correction factors to interpret the near/transition field data.

Anderson[14] reported the results on nonlinear least squares approach in the inversion of high frequency EM soundings. However, electromagnetic theory demands the employment of lower frequencies (often encroaching into near field conditions for finite source–receiver separation) to study deeper geoelectric layers. Thus it is necessary to evolve a suitable inversion scheme to obtain the geoelectric parameters from the near/transition field CSAMT data.

In this paper we address this important problem and study the feasibility of inverting near field CSAMT data observed over layered earth structure in terms of deeper geoelectric parameters.

Conventionally, the apparent resistivity as a function of frequency (f) is used to invert EM data to obtain the geoelectrical parameters. Apparent resistivity functions have also been discussed by several authors[15–19].

Figure 1 *a* shows Cagniard resistivity computed using the tangential electric (E_ϕ) and magnetic field (H_r) components of a vertical magnetic dipole (VMD) over homogeneous earth of conductivity (σ) (refs 20, 21).

$$E_\phi = i\omega\mu \frac{M}{4\pi r^2} e_\phi, \tag{1}$$

$$H_r = \frac{M}{4\pi r^3} h_r, \tag{2}$$

$$e_\phi = \frac{2}{p^2}[-3 + e^{ip}(3 - 3ip - p^2)], \tag{3}$$

$$h_r = \frac{-i\pi p^2}{2}\left[J_2\left(\frac{p}{2}\right)H_2\left(\frac{p}{2}\right) - J_1\left(\frac{ip}{2}\right)H_1\left(\frac{p}{2}\right)\right], \tag{4}$$

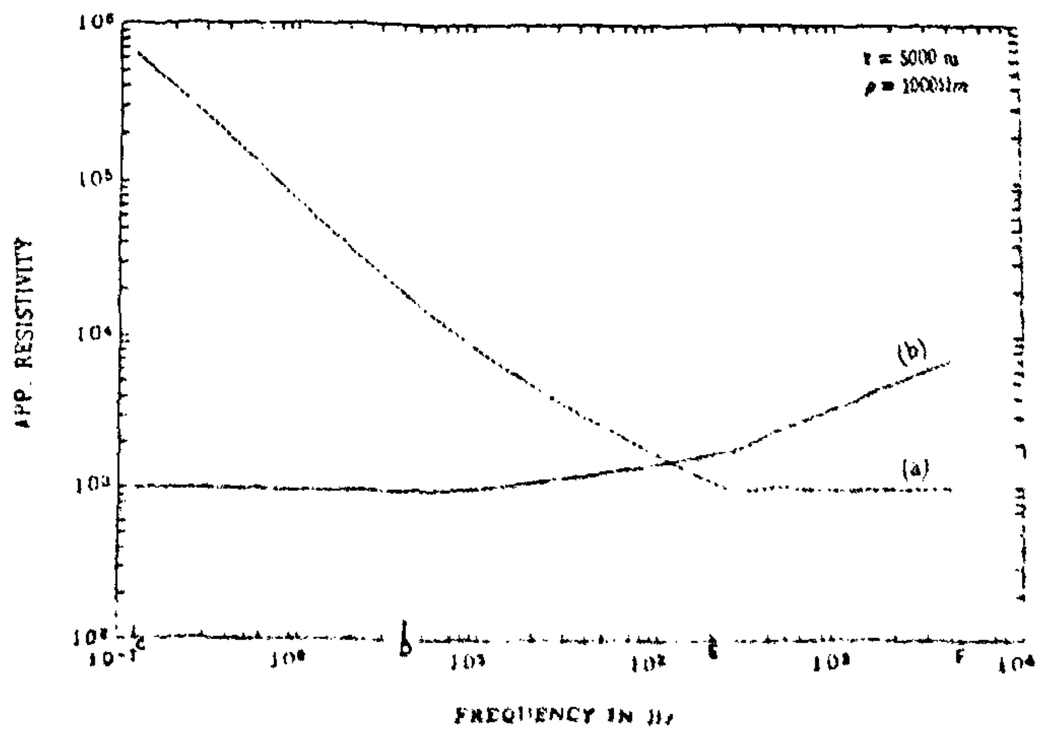

Figure 1. Far field and near field CSAMT responses for a homogeneous medium.

*For correspondence. (e-mail: ibrrrm@hd1.vsnl.net.in)

where $p = |\bar{k}r|$ and $\bar{k} = \sqrt{i\sigma\mu\omega}$, μ is the magnetic permeability, $\omega = 2\Pi f$, σ is the conductivity, f is frequency in Hertz, r is the transmitter–receiver distance, M is the magnetic moment of the dipole given by $M = ISn$, where I is the current in the loop, S is the area enclosed by the loop and n is the number of turns.

In the CSAMT technique, if the transmitter–receiver separation becomes less than 3 times the skin depth (skin depth $\delta = (2/\sigma\mu\omega)^{1/2}$ for a quasistatic case), the field becomes near field and the transmitter acts more like a local EM source rather than an MT source. Beyond 3 times the skin depth the field is called a 'far field'. Hence, measurements are made with frequencies in the near zone and are subjected to non plane wave effects causing a departure of Cagniard resistivity. In principle, this can be corrected on the basis of the field behaviour. Figure 8 of Rao *et al.*[3] defines the combination of r, f and σ for which near field (or far field) conditions are valid.

The segment EF of Figure 1 *a* is the far field response and is equal to the true resistivity of the homogeneous medium ($\rho = 1000$ Ohm m) that can be obtained from the Cagniard equation[22].

$$\rho_{\text{far}} = \frac{1}{\mu\omega}\left|\frac{E_\phi}{H_r}\right|^2, \tag{5}$$

when $|kr| \ll 1$, neglecting the higher order terms in eqs (3) and (4) we obtain

$$\left|\frac{e_\phi}{h_r}\right| = \frac{4}{p^2}. \tag{6}$$

Equations (1), (2) and (6) would yield

$$\rho_{\text{near}} = \frac{r}{4}\left|\frac{E_\phi}{H_r}\right|. \tag{7}$$

Figure 1 *b* shows near field apparent resistivity computed using eq. (7). As expected, segment CD in Figure 1 *b* yields the true resistivity of the homogeneous medium which possibly does not exist in Figure 1 *a* at the low frequency end of the spectrum. The points C and F indicate the frequency band used in the present study. Beyond E far field conditions are valid (for given σ and r), below D the near field conditions apply.

The electromagnetic field components for the multilayered earth due to a VMD source in the near zone are given by[23–25]:

$$E_\phi = \frac{-i\omega\mu M}{cr^2}e_\phi, \tag{8}$$

$$H_Z = \frac{-M}{r^3}h_Z, \tag{9}$$

$$H_r = \frac{-M}{r^3}h_r, \tag{10}$$

where c is the velocity of light, and e_ϕ, h_Z and h_r for the Kth layer are given by

$$e_\phi = 1 - \frac{1}{4}p_1^2\left[1 - \sum_{K=1}^{N-1}(\Gamma_K - \Gamma_{K+1})\left\{\sqrt{1+g_K^2} - g_K\right\}\right], \tag{11}$$

$$h_Z = 1 + \frac{1}{4}p_1\left[1 - \sum_{K=1}^{N-1}(\Gamma_K - \Gamma_{K+1})\frac{1}{\sqrt{1+g_K^2}}\right], \tag{12}$$

$$h_r = \frac{1}{4}p_1^2\left[1 - \sum_{K=1}^{N-1}(\Gamma_K - \Gamma_{K+1})\left\{\frac{g_K}{\sqrt{1+g_K^2}} - 1\right\}\right], \tag{13}$$

where $g_K = 2h_K/r$; $\Gamma_K = \sigma_K/\sigma_1$, σ_K and σ_1 are conductivities of the Kth layer and first-layer, respectively, for an N-layered earth.

Figure 2 *a* shows two-layer CSAMT response computed using the Cagniard resistivity and Figure 2 *b* is obtained by computing the apparent resistivity under near field conditions using the near field apparent resistivity for the same model. The model parameters and the experimental parameters are given in the figure. From Figure 2 *b* we see that it is possible to obtain the true resistivity of the substratum by using the near field solution and the near field definition of apparent resistivity, which is not possible in the conventional Cagniard resistivity computation since at low frequencies under these conditions the apparent resistivity increases with decrease in frequency, as in the case of a homogeneous medium.

We can also observe that the computed near field apparent resistivity approaches the true resistivity of the substratum for a particular combination of resistivity contrast and thickness to separation ratios. Figure 3 shows the

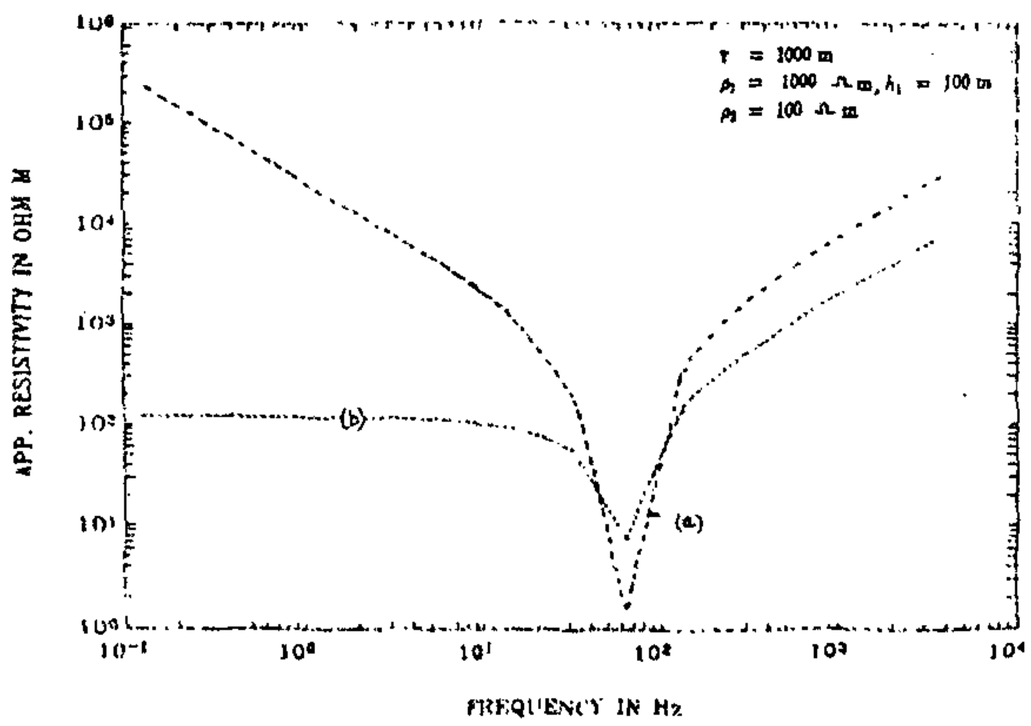

Figure 2. Far field and near field CSAMT responses for a two-layered medium.

relationship for a multitude of geoelectric parameters from which one can estimate the combinations of h_1/r and ρ_2/ρ_1, (where h_1 is the thickness, ρ_1 is the resistivity of the first-layer and ρ_2 is the resistivity of the substratum) for which the computed apparent resistivity approaches the true resistivity of substratum. For h_1/r values between 0.0005 and 0.002 the calculated points have been fitted graphically as some dispersion (though small) was observed (the actual points are marked in Figure 3). However, for h_1/r values between 0.002 and 0.01 no dispersion was observed. When the top layer is resistive compared to the substratum, say $\rho_1 = 300$ Ohm m and $\rho_2 = 100$ Ohm m such that $\rho_2/\rho_1 = 1/3$, a transmitter–receiver separation of 3.3 km would be required to obtain the true resistivity of the substratum when the first-layer thickness is 10 m.

Figure 4 shows a few near field CSAMT responses for a two-layered earth. The ratios ρ_2/ρ_1 and h_1/r determine the nearness of the low frequency segment of the apparent resistivity thus computed to the true resistivity of the basement. A general case requires inversion approach to retrieve the true geoelectrical parameters.

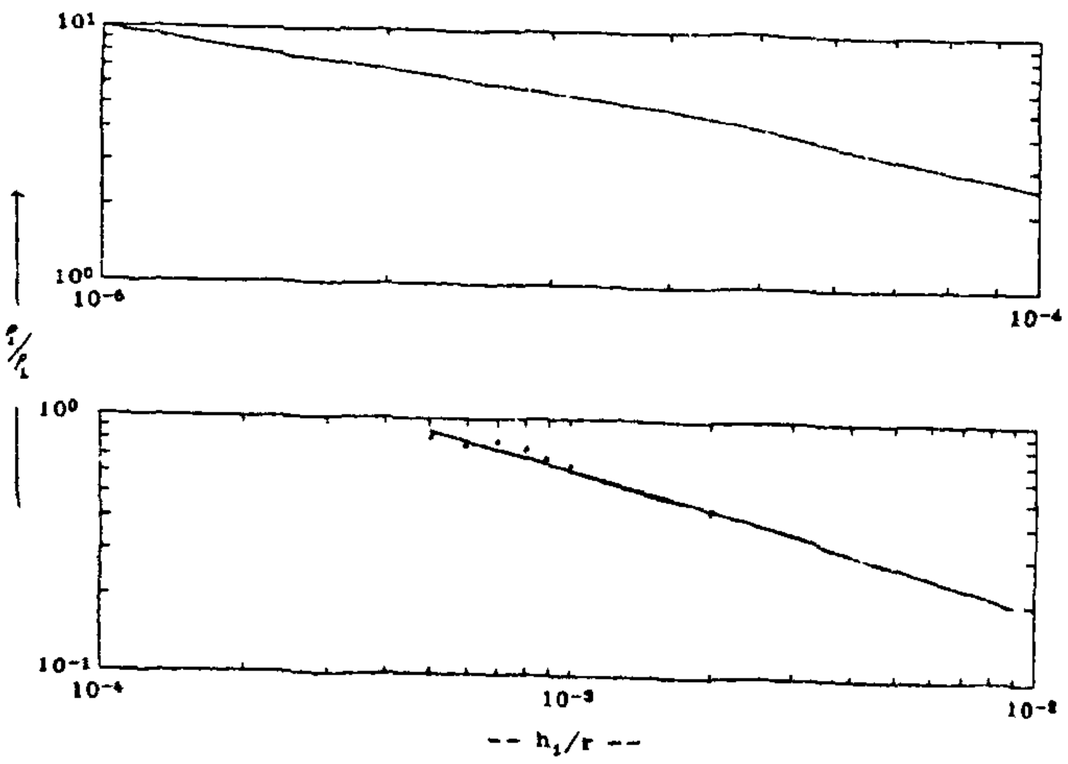

Figure 3. Nomogram for the parameters to obtain the true resistivity of the substratum for a two-layered earth.

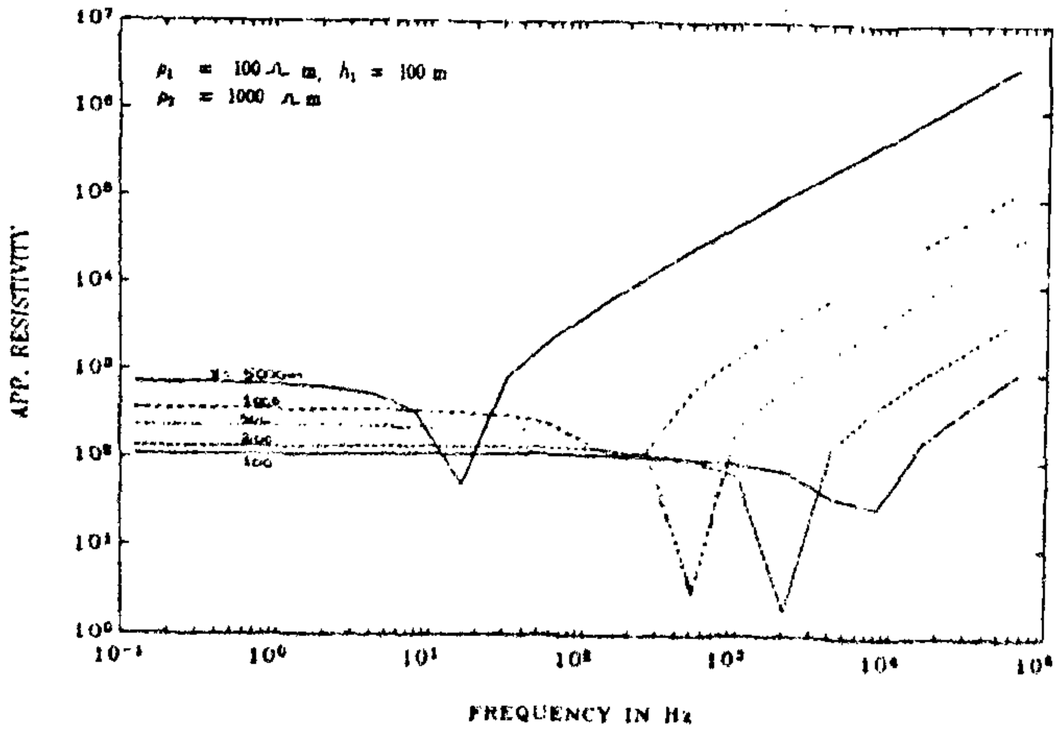

Figure 4. Near field CSAMT response over a two-layered earth for different transmitter-receiver separations.

We adopted the nonlinear least squares inversion[26] approach to invert the ρ_{near} function. Since the generalized linear inversion theory is well documented[27,28] and the EM forward problem can be linearized with the help of the Taylor's series expansion, we chose not to duplicate the same here. Likewise the nonlinear least squares inversion[26,29–32] is also not duplicated here. However, the logical flow of the interpretation scheme adopted is given in Figure 5 for the sake of comprehension. The forward problem solution is achieved through eq. (7) via eqs (8) and (10).

The proof of the efficacy of any inversion scheme lies in the agreement between the inverted parameters and the geological truth. Synthetic near zone CSAMT data generated are used as the input for the inversion technique developed. Table 1 shows two and three-layer geoelectrical models considered for generation of synthetic data in the present study. Cases 1 and 2 are two-layer models representing conductive and resistive basements, while cases 3–6 are A, K, H and Q-type three-layer models respectively.

Table 1. Two and three-layer models used in the present study

Model no.	ρ_1 Ohm m	ρ_2 Ohm m	ρ_3 Ohm m	h_1 (m)	h_2 (m)	r (m)
I (two-layer conductive basement)	1500	200	–	15	–	3000
II (two-layer resistive basement)	75	750	–	10	–	4000
III (three-layer A-type)	50	150	500	130	20	300
IV (three-layer K-type)	500	150	50	130	20	300
V (three-layer H-type)	50	10	500	130	20	300
VI (three-layer Q-type)	50	150	50	130	20	300

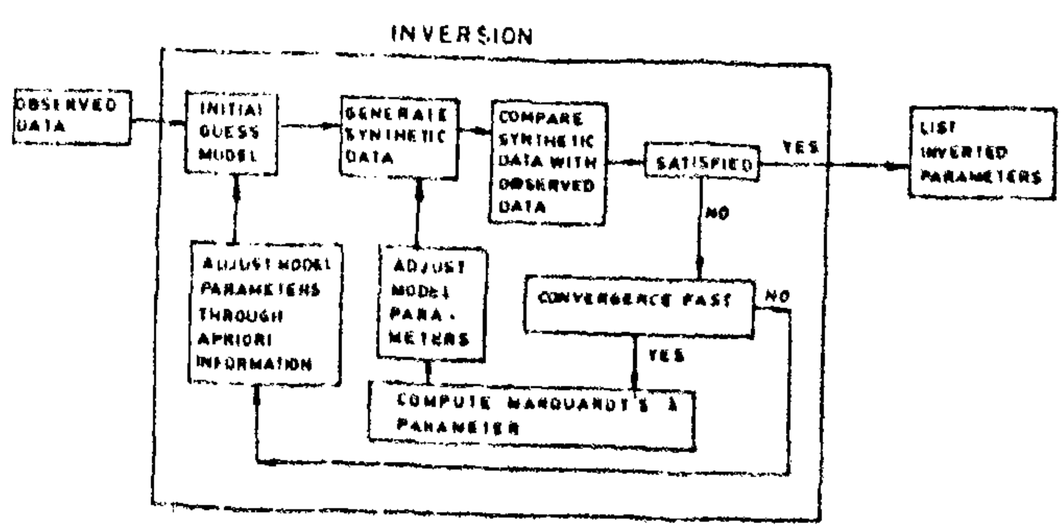

Figure 5. Schematic diagram depicting the inversion process developed.

An initial guess model was chosen such that it deviated at least by 20% from the true parameters. Figures 6 and 7 show the results obtained from the inversion scheme developed for two-layer geoelectric models. Tables 2 and 3 show the iteration steps along with the deviation in per cent ($\varepsilon\%$) between the response obtained from the true parameters (F_i) and that obtained from each iteration (Y_i). $\varepsilon\%$ for L different frequencies and N layers is given by

$$\varepsilon\% = \sqrt{\frac{1}{L-(2N-1)}\sum_{i=1}^{L}[D_i - Y_i]^2} \times 100.$$

A similar scheme of inversion is adopted for the three-layered earth model. Figures 8 and 9 show a few results obtained for various three-layer model parameters. The results are shown in Tables 4 and 5 respectively.

Table 2. Results of iteration process for two-layer model

Actual parameters
$r = 300$ m;
$\rho_1 = 1500$ Ohm m; $\rho_2 = 200$ Ohm m; $h_1 = 15$ m

Initial guess model
$\rho_1 = 1900$ Ohm m; $\rho_2 = 250$ Ohm m; $h_1 = 19$ m

Inverted parameters

Iteration no.	ρ_1	ρ_2	h_1	$\varepsilon\%$
1	1899.99	201.024	18.4	1.948
2	1899.99	199.93	15.13	0.0028
3	1899.99	199.97	14.77	5.64×10^{-7}

Table 3. Results of iteration process for two-layer model

Actual parameters
$r = 4000$ m;
$\rho_1 = 75$ Ohm m; $\rho_2 = 750$ Ohm m; $h_1 = 10$ m

Initial guess model
$\rho_1 = 50$ Ohm m; $\rho_2 = 500$ Ohm m; $h_1 = 5$ m

Inverted parameters

Iteration no.	ρ_1	ρ_2	h_1	$\varepsilon\%$
1	80.66	751.852	19.51	424.021
2	82.706	751.45	12.599	3.9432
3	81.44	748.99	10.62	0.0252
4	81.349	748.57	10.46	1.02×10^{-6}

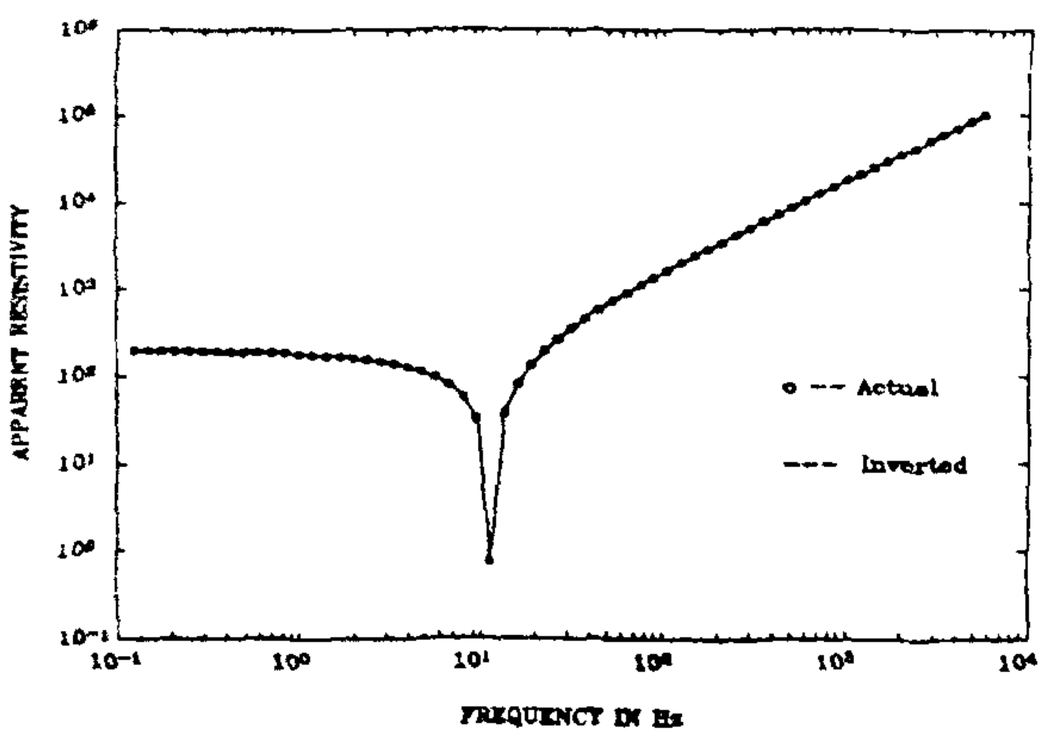

Figure 6. *Results of the inversion scheme of a two-layer CSAMT response for the parameters shown in Table 2.*

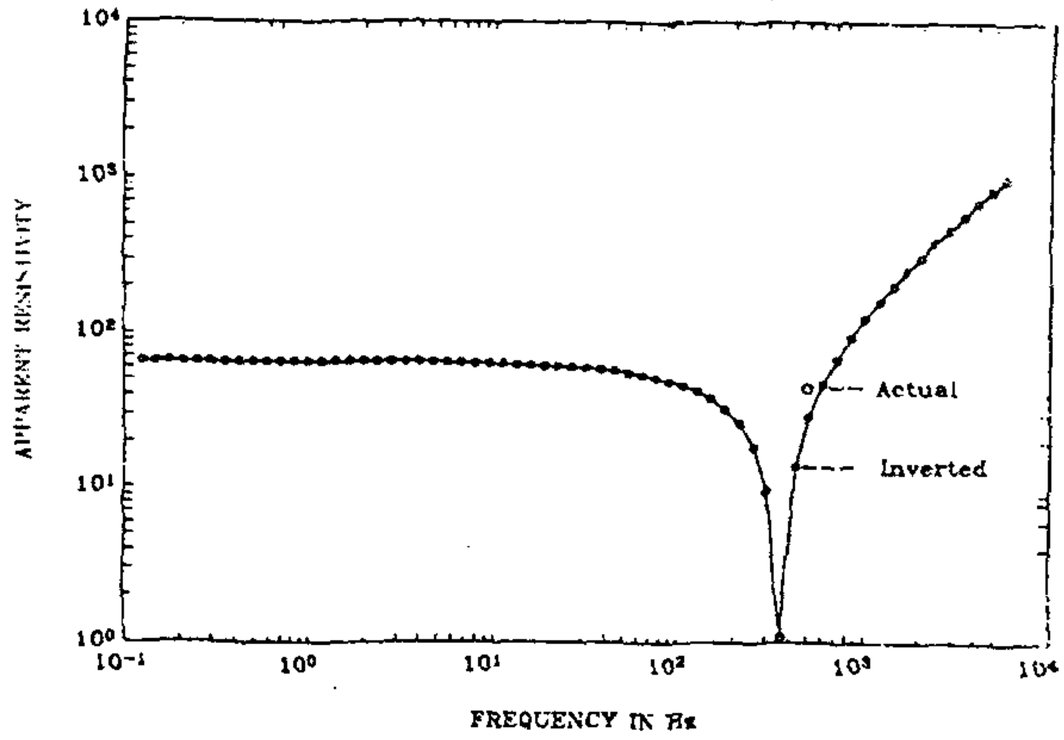

Figure 8. *Results of the inversion scheme of a two-layer CSAMT response for the parameters shown in Table 4.*

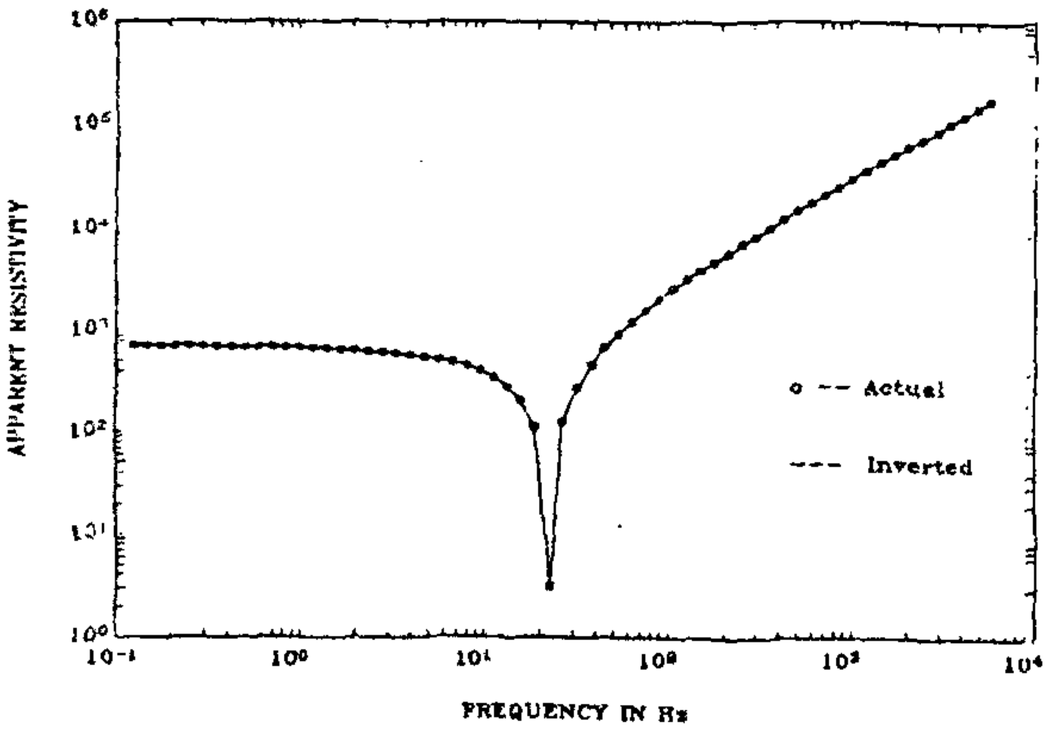

Figure 7. Results of the inversion scheme of a two-layer CSAMT response for the parameters shown in Table 3.

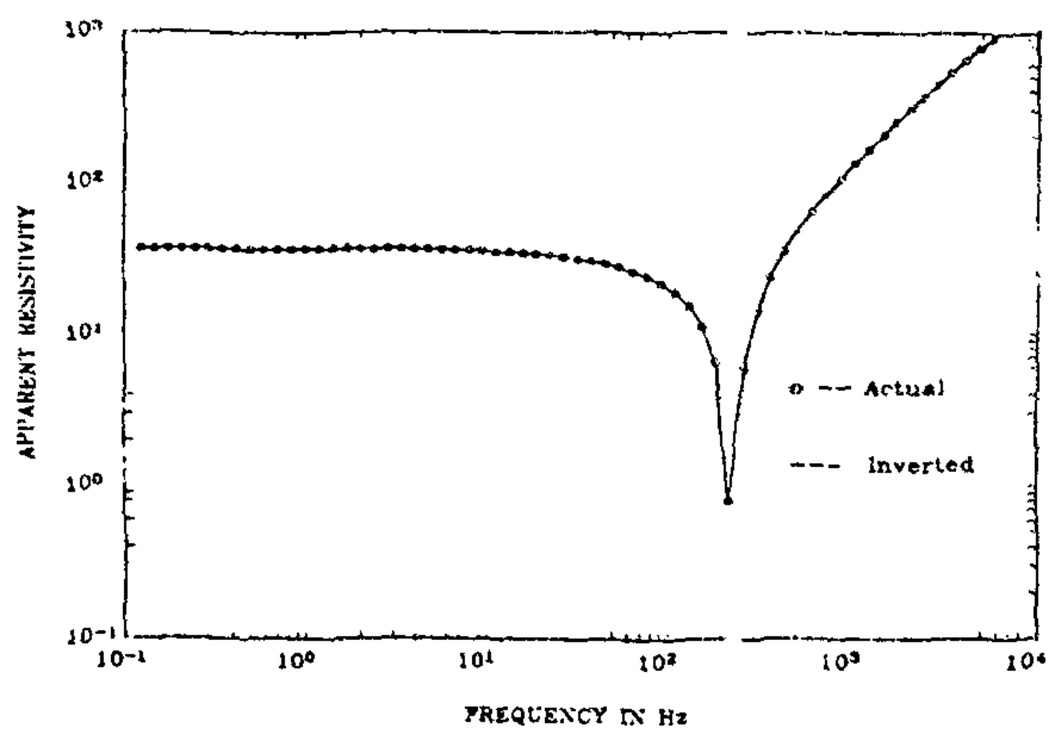

Figure 9. Results of the inversion scheme of a two-layer CSAMT response for the parameters shown in Table 5.

Though in principle it is possible to skip the intermediate iteration steps and fix a limit to the error for terminating the iteration process, the intermediate steps of iteration are shown to appreciate the convergence. Within a reasonable number of iterations the final geoelectrical parameters obtained matched reasonably well with the true parameters. However, when dealing with real data such fast convergence may not be possible due to the presence of 'noise'.

The determined states of the object from the field measurements using any inversion scheme are characterized by a natural probability distribution. Their effectiveness is given by the Covariance Matrix (CV) (obtained by inverting the information matrix) whose diagonal elements represent the scatter of the inverted results around the truth[33,34]. Ideally CV does not depend on the experimental parameters[33]. Glenn *et al.*[28] present the parameter resolution obtained from the information density matrix, as a function of each iteration for a fixed separation.

It is possible to generate a number of synthetic data from the observed data by say Monte Carlo simulation. Statistical properties of the difference between the inverted parameters obtained from the observed data and synthetic data provide an estimate of the efficacy of the scheme[35].

The success of any inversion scheme depends on strict adherence to fulfillment of the conditions governing the forward problem solution and may depend on experimental parameters also when such an adherence is not guaranteed. Thus, in order to estimate the accuracy, we applied this scheme to a multitude of geoelectric truths and transmitter–receiver separations within the frequency range of 0.125 Hz to 4 kHz for both two and three-layer geoelectric models. We studied the per cent deviation of the inverted geoelectrical parameters from their true values which is of greater significance in any data acquisition/inversion cycle, especially when the initial conditions cannot be rigidly adhered to in practice.

The per cent deviation in the depth and resistivity parameters was estimated as

$$\Delta\alpha\% = \frac{\alpha_{\text{true}} \sim \alpha_{\text{inv}}}{\alpha_{\text{true}}} \times 100,$$

where α is the representative value of either the depth (H) or resistivity (ρ). Tables 6 and 7 show a few results obtained from the inversion scheme for two and three-layer geoelectrical models, respectively along with $\Delta\alpha\%$. Figure 10 shows $\Delta\alpha\%$ as a function of (ρ_2/ρ_1) for various r/h_1 values in the case of a two-layer geoelectric section. As the resistivity of the substratum increases (for $(\rho_2/\rho_1) < 1$) the error steeply increases (for small values of ρ_2/ρ_1) for all values of r/h_1 (Figure 10 *a*). However, for large values of r when compared to the first-layer thickness the error obtained is well below 15% within the range of resistivity parameters investigated (Figure 10 *a*). On the other hand, when ρ_2 is more than 20 times ρ_1 and when r/h_1 is greater than or equal to 1 the error is well within 5% (Figure 10 *b*). However, even in this case if ρ_2 is less than 20 times ρ_1 the error in the inverted parameter is much higher. Further, when r is less than h_1 the error exceeds 5% within the range of resistivity parameters investigated. Thus, a satisfactory solution can be expected from the scheme developed when ρ_2/ρ_1 is greater than or equal to 20 and r/h_1 is greater than or equal to unity.

Table 4. Results of iteration process for three-layer model

Actual parameters
$r = 300$ m;
$\rho_1 = 50$ Ohm m; $\rho_2 = 150$ Ohm m; $\rho_3 = 50$ Ohm m
$h_1 = 130$ m; $h_2 = 20$ m

Initial guess model
$\rho_1 = 60$ Ohm m; $\rho_2 = 180$ Ohm m; $\rho_3 = 60$ Ohm m
$h_1 = 155$ m; $h_2 = 24$ m

Inverted parameters

Iteration no.	ρ_1	ρ_2	ρ_3	h_1	h_2	$\varepsilon\%$
1	56.587	180.218	49.25	155.459	22.96	0.036
2	55.97	180.27	49.39	155.52	22.092	1.74×10^{-6}

Table 5. Results of iteration process for three-layer model

Actual parameters
$r = 300$ m;
$\rho_1 = 500$ Ohm m; $\rho_2 = 150$ Ohm m; $\rho_3 = 50$ Ohm m
$h_1 = 130$ m; $h_2 = 20$ m

Initial guess model
$\rho_1 = 400$ Ohm m; $\rho_2 = 120$ Ohm m; $\rho_3 = 40$ Ohm m
$h_1 = 105$ m; $h_2 = 16$ m

Inverted parameters

Iteration no.	ρ_1	ρ_2	ρ_3	h_1	h_2	$\varepsilon\%$
1	400.037	119.711	50.46	105.155	17.519	0.0645
2	400.047	119.60	50.26	105.24	17.632	3.44×10^{-8}

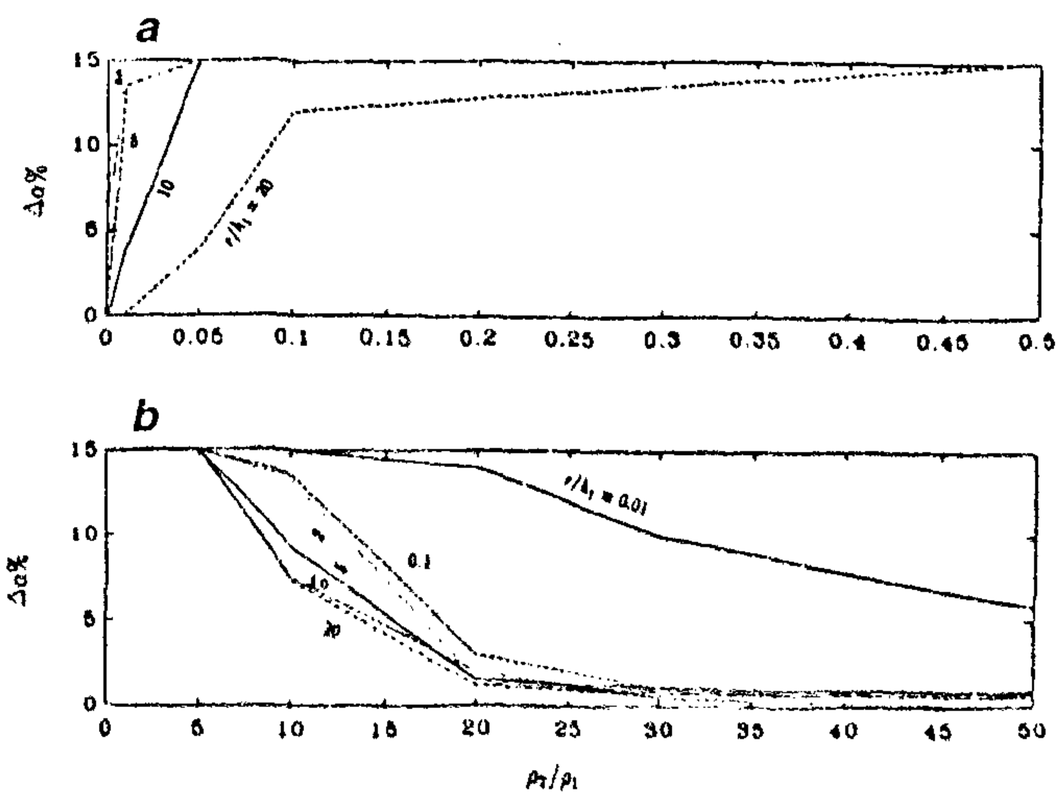

Figure 10. $\Delta\alpha\%$ nomogram for a two-layered earth model.

Since the $\Delta\alpha\%$ in the case of apparent resistivity was found to follow very closely the $\Delta\alpha\%$ for the depth parameter, no separate discussion is presented.

In order to test the robustness of the approach for grappling with the near field CSAMT data, the synthetic CSAMT data were corrupted with 5% random noise. For this purpose models II and IV from Table 1 (depicting two and three-layered models) were chosen. The noise was added to each observation randomly and the data thus obtained were used as the input.

Table 8 shows the results of inversion of the random noise corrupted data. For model II, where the basement is highly resistive $(\rho_2/\rho_1) > 1$, $\Delta\alpha\%$ is large for h_1, which is similar to the case when the data are not corrupted by random noise (Figure 10). However, a comparison of Tables 6 and 7 (without noise) with Table 8 (with noise)

Table 6. Results of inversion without random noise

	True resistivities			Guess inputs			Fitted resistivities			$\Delta\alpha\%$		
Model no.	ρ_1	ρ_2	ρ_3	ρ_1	ρ_2	ρ_3	ρ_1	ρ_2	ρ_3	ρ_1	ρ_2	ρ_3
I	1500	200	–	1900	250	–	1899.99	199.97	–	20.00%	0.02%	–
				1100	150	–	1100.00	200.50	–	20.00%	0.25%	–
II	75	750	–	50	500	–	81.35	748.57	–	8.47%	0.19%	–
				100	1000	–	19.84	786.09	–	73.55%	4.81%	–
III	50	150	500	40	120	400	46.28	123.86	413.00	7.44%	18.43%	17.40%
				60	180	600	54.92	137.25	569.16	9.84%	8.50%	13.83%
IV	500	150	50	400	120	40	400.94	119.60	50.26	20.00%	20.00%	0.52%
				600	180	60	599.98	50.26	49.54	20.00%	20.00%	1.00%
V	50	10	500	40	8	400	39.60	8.30	399.59	21.00%	17.00%	20.00%
				60	12	600	60.00	11.00	599.99	20.00%	10.00%	20.00%
VI	50	150	50	40	120	40	42.09	119.89	51.52	15.82%	20.07%	3.04%
				60	180	60	55.97	180.27	49.39	11.94%	20.18%	1.22%

Table 7. Results of inversion without random noise

	True thickness			Guess inputs			Fitted thickness			$\Delta\alpha\%$		
Model no.	h_1	h_2	H	h_1	h_2	H	h_1	h_2	H	h_1	h_2	H
I	15	–	15	19	–	19	14.77	–	14.77	1.53%	–	1.87%
				11	–	11	15.41	–	15.41	2.73%	–	2.73%
II	10	–	10	5	–	5	10.46	–	10.46	4.60%	–	4.60%
				15	–	15	4.93	–	4.93	50.70%	–	50.7%
III	130	20	150	105	16	121	131.0	0.011	131.01	0.77%	100.00%	12.66%
				155	24	179	186.63	29.88	216.51	43.56%	49.40%	44.34%
IV	130	20	150	105	16	121	105.24	17.63	122.87	20.00%	11.75%	18.08%
				155	24	179	154.9	22.89	177.79	20.00%	14.45%	18.53%
V	130	20	150	105	16	121	105.4	18.97	124.37	20.00%	5.150%	17.09%
				155	24	179	155.0	24.14	179.14	20.00%	20.00%	19.43%
VI	130	20	150	105	16	121	104.97	17.34	122.31	20.00%	13.30%	18.46%
				155	24	179	155.52	22.09	177.61	20.00%	10.00%	18.41%

Table 8. Results of inversion with random noise corrupted data

	Actual model parameters			Initial guess parameters			Fitted parameters			$\Delta\alpha\%$		
Model no.	ρ_1	ρ_2	ρ_3	ρ_1	ρ_2	ρ_3	ρ_1	ρ_2	ρ_3	ρ_1	ρ_2	ρ_3
II	75	750	–	50	500	–	43.75	812.78	–	42.0%	8.4%	–
IV	500	150	50	400	120	40	399.966	120.481	50.406	20.0%	20.0%	0.81%
	h_1	h_2	H	h_1	h_2	H	h_1	h_2	H	h_1	h_2	H
II	10	–	10	5	–	5	17.71	–	17.71	77.1%	–	77.10%
IV	130	20	150	105	16	121	104.556	16.176	120.732	20.0%	19.0%	19.50%

revealed that when the noise is present, the efficacy of the scheme deteriorated for model II. In the case of model IV when $(\rho_2/\rho_1) < 1$, $\Delta\alpha\%$ for all the parameters is nearly the same as that obtained for the data not corrupted by random noise.

There appears to be a way out to invert the near zone CSAMT data which is a necessity to probe deeper layers. The scheme presented can be extended to multi-layer sections without much difficulty. However, the case of resistive substratum (two-layer or A-type three-layer model) appears to have poorer resolvability in view of large errors in $\Delta\alpha\%$ for depth factor (Tables 7 and 8).

1. Yamashita, M. and Hallof, P. G., CSAMT case histories with a multichannel CSAMT system and discussion of near field data correction, Phoenix Geophysics Limited, Markham, 1985.
2. Zonge, K. L. and Hughes, J. L., *CSAMT, E.M. Methods in Applied Geophysics* (eds Nabighian, M. N.), Society of Exploration Geophysicists, 1991, vol. 2, p. 713–809.
3. Rao, I. B. R., Ram Raj Mathur and Srinivas, S., *Curr. Sci.*, 1994, **67**, 446–453.
4. Sandberg, S. K. and Hohmann, G. W., *Geophysics*, 1982, **47**, 100.
5. Boerner, D. E., Wright, J. A., Thurlow, J. G. and Reed, L. E., *Geophysics*, 1993, **58**, 12–19.
6. Sasaki, Y., *Geophysics*, 1989, **54**, 254–262.
7. Sasaki, Y., Yoneda, Y. and Matsuo, K., *Geophysics*, 1992, **57**, 952–955.
8. Takakura, S., *Explor. Geophys.*, 1995, **26**, 172–178.
9. Ogawa, Y. and Takakura, S., *J. Geomagn. Geoelectr.*, 1990, **42**, 211–224.
10. Yamashita, M., Controlled Source Audio Magnetotellurics Field Survey Results, Phoenix Geophysics Limited, Markham, 1987.
11. Bromley, C., *J. Geomagn. Geoelectr.*, 1993, **45**, 887–896.
12. Pris, G. V. and Svetov, B. S., *Appl. Geophys.* (in Russian), 1970, **59**, 92–102.
13. Bartel, C. and Jacobson, R. D., *Geophysics*, 1987, **52**, 665–677.
14. Anderson, W. L., *Geophysics*, 1991, **56**, 1087–1092.
15. Wilt, M. and Strak, M., *Geophysics*, 1982, **47**, 1100–1105.
16. Spies, B. R. and Eggers, D. E., *Geophysics*, 1986, **51**, 1452–1471.
17. Basokur, A. T., *Geophys. Prospect.*, 1994, **42**, 141–147.
18. Szarka, L., *Geophys. Prospect.*, 1994, **42**, 987–988.
19. Das, U., *Geophysics*, 1995, **60**, 53–60.
20. Kaufman, A. A. and Keller, G. V., *Frequency and Transient Soundings*, Elsevier Science Publishers, Amsterdam, 1983.
21. Khmelovsky, G. V. and Bondarenko, V. M., *Electrical Prospecting, Hand Book of Geophysics*, Nedra, Moscow, 1989.
22. Cagniard, L., *Geophysics*, 1953, **18**, 605–635.
23. Gasanenko, L. B. and Sholpo, G. P., *Problems in Geophysics* (in Russian), Leningrad University Publications, 1959, p. 174–183.
24. Gasanenko, L. B., *Problems in Geophysics* (in Russian), Leningrad University Publications, 1960, p. 286.
25. Svetov, *Theory, Methodology and Interpretation of Low Frequency Inductive Electrical Prospecting Data* (in Russian), Nedra, Moscow, 1973.
26. Marquardt, D. W., *J. Soc. Ind. Appl. Math.*, 1963, **11**, 431–441.
27. Wiggins, R. A., *Rev. Geophys. Space Phys.*, 1972, **10**, 251–286.
28. Glenn, W. E., Ryu, Jisoo, Ward, S. H., Peoples, W. J. and Phillips, R. J., *Geophysics*, 1973, **38**, 1109–1129.
29. Marquardt, D. W., *Technometrics*, 1970, **12**, 591–612.
30. Daniels, J. J., Keller, G. V. and Jacobson, J. J., *Geophysics*, 1976, **41**, 752–765.
31. Anderson, W. L., USGS Open-file Report, 1979, **37**, 79–586.
32. Anderson, W. L., USGS Open-file Report, 1982, **65**, 68–82.
33. Goldtzman, F. M., *Izv. Earth Phys.*, 1975, **29**, 53.
34. Jenkins, G. M. and Watts, D. C., *Spectral Analysis and Its Applications*, Holden-day, Inc., 1968.
35. Press, W. H., Teukolsky, S. A., Vellerling, W. T. and Flannery, B. P., *Numerical Recipes in Fortran*, Cambridge University Press, Cambridge, UK, 1992.

ACKNOWLEDGEMENTS. We gratefully acknowledge many positive suggestions of the anonymous reviewer. We thank DST, Government of India for financial assistance.

Received 7 April 1999; revised accepted 3 November 1999

Clinopyroxenite xenoliths from the Deccan Trap lavas of Kutch and Mumbai

D. Chandrasekharam* and K. C. Vinod

Department of Earth Sciences, Indian Institute of Technology, Powai, Mumbai 400 076, India

Only a few occurrences of mantle xenoliths have been reported in the Deccan basalt province. These include the spinel peridotite and spinel lherzolite from Kutch and clinopyroxenite (with minor olivine) from Murud–Janjira coast. We now report hitherto unknown clinopyroxenite xenoliths from Kutch and Powai. The Kutch xenoliths are accidental and the Powai xenoliths are cognate. The Kutch clinopyroxenite xenoliths appear to have been formed due to the reaction between the mantle, containing olivine and orthopyroxene, and carbonated alkaline magma at about 1100°C and 17 kb pressure. The Powai xenolith represents cumulates of clinopyroxenes in the magma chamber which were picked up and brought up by a subsequent eruption.

IN the vast Deccan flood basalt province of India, mantle xenoliths are quite rare. However, a few occurrences of mantle xenoliths are known in the province[1–5]. The xenoliths in alkali olivine basalts from Kutch, Gujarat comprise dunites, spinel peridotites[4] and spinel lherzolites[3]. Xenoliths of clinopyroxenites (with minor olivine) are found in the lamprophyre dykes of Murud–Janjira along the western coast of India [1,5]. We report here, two hitherto unknown types of xenoliths, namely clinopyroxenite xenoliths from the alkali olivine basalts of Dhrubiya and Nana, Kutch (Figure 1 *a*) and also from the tholeiitic basalts of Powai, Mumbai (henceforth termed as 'campus xenoliths'; Figure 1 *b*) and discuss in detail their petrographic characteristics.

The alkali olivine basalts of Kutch containing the xenoliths have been dated at about 64 Ma (ref. 4). The

*For correspondence. (e-mail: dchandra@geos.iitb.ernet.in)